

# Hamiltonian Learning with Online Bayesian Experiment Design in Practice

Ian Hincks,<sup>1,2</sup> Thomas Alexander,<sup>3,2</sup> Michal Kononenko,<sup>2,4</sup> Benjamin Soloway,<sup>2,5</sup> and David G. Cory<sup>6,2,7,8</sup>

<sup>1</sup> Department of Applied Mathematics, University of Waterloo, Waterloo, ON, Canada

<sup>2</sup> Institute for Quantum Computing, University of Waterloo, Waterloo, ON, Canada

<sup>3</sup> Department of Physics, University of Waterloo, Waterloo, ON, Canada

<sup>4</sup> Department of Chemical Engineering, University of Waterloo, Waterloo, ON, Canada

<sup>5</sup> Department of Physics and Astronomy, Haverford College, Haverford, PA, United States

<sup>6</sup> Department of Chemistry, University of Waterloo, Waterloo, ON, Canada

<sup>7</sup> Perimeter Institute for Theoretical Physics, 31 Caroline St. N, Waterloo, Ontario, Canada N2L 2Y5

<sup>8</sup> Canadian Institute for Advanced Research, Toronto, ON, Canada

(Dated: June 8, 2018)

Estimating parameters of quantum systems is usually done by performing a sequence of pre-determined experiments and post-processing the resulting data. It is known that online design, where the choice of the next experiment is based on the most up-to-date knowledge about the system, can offer speedups to parameter estimation. We apply online Bayesian experiment design to a Nitrogen Vacancy (NV) in diamond to learn the values of a five-parameter model describing its Hamiltonian and decoherence process. Comparing this to standard pre-determined experiment sweeps, we find that we can achieve median posterior variances on some parameters that are between 10 and 100 times better given the same amount of data. This has applications to NV magnetometry where one of the Hamiltonian coefficients is the parameter of interest. Furthermore, the methods that we use are generic and can be adapted to any quantum device.

## I. INTRODUCTION

Characterizing quantum devices efficiently is an increasingly important problem. In the case of quantum processors, knowing system properties and error processes is helpful for designing robust high-fidelity control. If system parameters drift in time, they will need to be periodically recharacterized, which reduces uptime. Or, in the case of metrology, certain properties of the quantum system are themselves the quantities of interest, and so more efficient characterization leads to higher sensitivities.

Quantum system characterization is typically done by performing a set of predetermined experiments and subsequently processing statistics of the resulting data. While there is nothing wrong with this—and indeed, in some cases, this strategy can even be tuned to have near optimal performance—it has long been known that *online* (also called *adaptive* by some authors) experiment design is generally capable of outperforming predetermined experiment sweeps [1, 2]. As its name implies, online experiment design allows the next experiment choice to depend somehow on what has already been learned. The reason for the advantage is obvious—online experiments can potentially avoid executing experiments that are expected to be uninformative by using information that was initially unavailable.

Online experiment design has a long history in quantum systems. Almost five decades ago, it was used to reduce the time required to determine relaxation rates in NMR spin systems [3], and later to speed up inversion recovery  $T_1$  measurements [4]. In recent decades, it has been studied extensively, both in theory and experiment, in the context of quantum phase estimation [2, 5–11] and quantum state tomography [12–18]. Online experiment

design has been suggested for sequence length choices in randomized benchmarking experiments[19], and adaptive protocols to generate control pulses for quantum systems have been proposed [20–22]. Here we build on online experiment design applied to quantum Hamiltonian estimation [23–28], where a Hamiltonian form (or set of forms) is specified, and unknown coefficients of Hamiltonian terms are sought.

The purpose of the present work is to study online Bayesian experiment design, with Hamiltonian estimation as the inference problem of choice, using experimental data and noise on a system with slightly non-trivial dynamics. By non-trivial we mean that there are more than one or two relevant inference parameters (we ultimately use 10, including nuisance parameters describing optical drift), that quantum state evolution does not admit a nice closed form solution, and that we allow the ability to turn on and off the control field within an experiment. In doing so we hope to pave the way for similar experiments in yet more complex systems. To this end we interface a sequential Bayesian inference engine with an experimental setup that controls the qutrit manifold of a single Nitrogen Vacancy (NV) defect in diamond. NV defects are widely studied quantum systems that can be initialized and read-out optically [29–31], manipulated at microwave frequencies[32], and have long coherence times at room temperature[33]. Their proposed applications include quantum sensing [34–36] and building quantum repeaters[37].

This paper proceeds as follows. In Section II we briefly overview statistical inference, followed by a short summary of Bayesian experiment design in Section III. In Section IV we define a system model for the NV system in particular, whereas the previous sections were general. In Section V we discuss some hardware, software, and im-

plementation details of our setup. Finally, in [Section VII](#) we present our results comparing offline and online experiment design heuristics. Code and data to reproduce the results of this paper can be found in Reference [\[38\]](#).

## II. INFERENCE OF QUANTUM DEVICES

We begin by defining some notation while reviewing parameter estimation as applied to quantum devices.

Information about a quantum device can be encoded into a list of real values, which we call *model parameters*, labeled  $x$ . For example, in the case of Hamiltonian learning, these values parameterize the Hamiltonian operator of the quantum system, or in the case of state tomography, the entries of a density operator. This set of parameters includes both parameters of interest, which one is interested in learning, and nuisance parameters, which are not of principle interest, but are still necessary to sufficiently describe the system.

Quantum devices are controlled by some collection of classical knobs that adjust various settings such as power, timings, carrier frequencies, and so on. We refer to a specific assignment of all of these settings as an *experiment configuration*, sometimes called the control variables, which we label  $e$ . Then an *experiment* consists of a quantum measurement (or set of quantum measurements) made using this fixed experiment configuration. For example, in this nomenclature, a standard Rabi curve would be constructed by making a set of experiments, each one defining—among other fixed parameters—a pulsing time in its experimental configuration,  $e = (\dots, t_{\text{pulse}}, \dots)$ .

An experiment returns a datum  $d$ . This might be a photon count over a known time interval, a time series of voltages, or a number of ‘down’ strong measurement results out of  $N$  repetitions, and so on.

Generally, the goal of statistical inference is to learn the parameters  $x$  given a data set  $d_1, \dots, d_n$  with respective configurations  $e_1, \dots, e_n$ . This requires us to additionally specify a model for the system—something which connects the model parameters to the experiment configurations and data. This is done through a likelihood function,

$$L(x; d_{1:n}, e_{1:n}) = \Pr(d_{1:n}|x, e_{1:n}), \quad (1)$$

which returns the probability of receiving a given dataset conditioned on a hypothetical configuration  $x$ . Here, and throughout this paper, we use subscripted index-range notation, where, for example,  $d_{1:n} = \{d_1, \dots, d_n\}$ . Note that multiple models can be considered and compared—known as model selection—if the true model is not known. For quantum systems, these likelihood models come naturally through quantum system evolution formulas in conjunction with Born’s rule.

One popular inference choice is to maximize the likelihood function with respect to  $x$ , producing the maximum

likelihood estimate (MLE)  $\hat{x}_{\text{MLE}} := \operatorname{argmax}_x L$ . Confidence regions of this estimate can be constructed with statistical derivations, or more generally, through techniques like bootstrapping. Least-squared curve fitting is often used as a proxy for the MLE (with confidence intervals arriving from assuming a linearized model) since it is exactly equal to the MLE for linear models and normal likelihood functions.

The MLE is one example of an estimator in a vast literature on estimator theory. In the present work, we limit ourselves to the use of Bayesian inference because of its natural integration with online experiments, discussed below. In short, in the paradigm of (sequential) Bayesian inference, one maintains the most current state of knowledge about the model parameters  $x$ , encoded as a probability distribution  $\pi_n(x) = \Pr(x|d_{1:n}, e_{1:n})$ , where  $n = 1, 2, 3, \dots$  indexes the state of knowledge when the first  $n$  data points  $d_{1:n}$  have been collected and processed from the first  $n$  experiments  $e_{1:n}$ . We write  $\pi_0(x)$  to denote the distribution prior to all measurements. The update from  $\pi_{n-1}$  to  $\pi_n$  is done through Bayes’ law,

$$\pi_n(e) = \frac{\Pr(d_n|x, e_n)\pi_{n-1}(x)}{\Pr(d_n|e_n)}, \quad (2)$$

so that our knowledge is improved sequentially as each datum arrives. Note that the chain rule of conditional probabilities can be used to expand this equation into  $\pi_n(e) = \Pr(d_{1:n}|x, e_{1:n})\pi_0(x)/\Pr(d_{1:n}|e_{1:n})$ .

## III. BAYESIAN EXPERIMENTAL DESIGN

An *experiment design heuristic* is simply a function that determines the next experiment configuration to use. We say such a heuristic is *online* if it explicitly uses the results of preceding experiments, and we call it *offline* otherwise. An experiment design timing diagram is shown in [Figure 1](#). Conventionally, as an example, Rabi curves are generated with offline heuristics, where the next experiment is chosen by increasing the pulse time by a fixed duration in each experiment. The number of experiments and pulse time increments are usually chosen through Nyquist considerations based on prior implicit beliefs about the frequencies and relaxation times of the system.

We restrict our online design heuristics to Bayesian designs, summarized in the following framework. Let  $U_n(x, d, e)$  be the utility of collecting the datum  $d$  under configuration  $e$  given the hypothetical model parameters  $x$  and the current state of knowledge  $\pi_n(x)$ , where a large value is good. Using the Bayesian maxim of marginalizing over unknown quantities, the average utility of observing  $d$  at step  $n + 1$  under the possible experiment configuration  $e$  is

$$U_n(d, e) = \int \tilde{\pi}_{n,d,e}(x)U_n(x, d, e)dx. \quad (3)$$

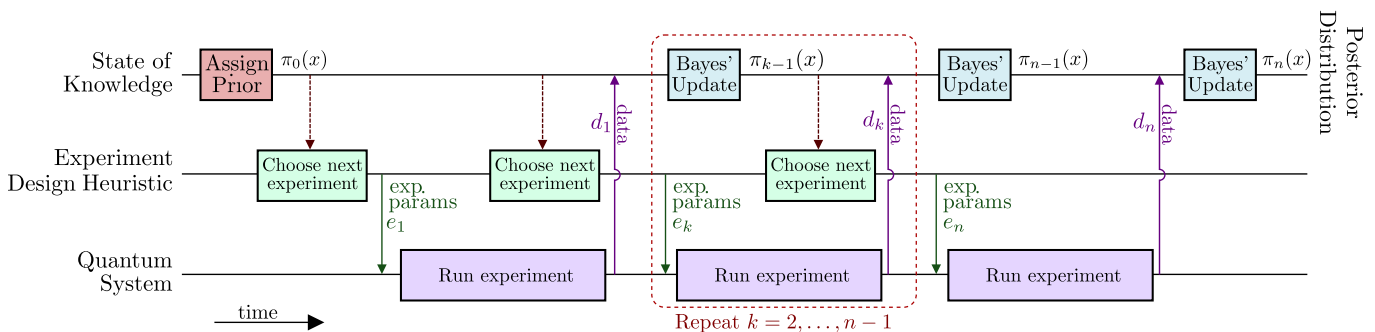


Figure 1: Timing diagram of online Bayesian learning. The role of the experiment design heuristic is to pick the next experiment configuration  $e_{n+1}$ , possibly based on the current state of knowledge,  $\pi_n(x)$ , resulting in the new data point  $d_{n+1}$ . This choice of experiment is computationally expensive, and is therefore run concurrently with quantum experiments.

where  $\tilde{\pi}_{n,d,e}(x) \propto L(x; d, e)\pi_n(x)$  is the hypothetical posterior at step  $n + 1$  assuming  $d$  will be observed. Since we do not know *a priori* which  $d$  will occur, the average utility of the possible configuration  $e$  as a whole is

$$U_n(e) = \int \Pr(d|e)U_n(d, e)dd. \quad (4)$$

where  $\Pr(d|e) = \int \Pr(d|x, e)\pi_n(x)dx$  is the predictive distribution<sup>1</sup>. Based on this quantity we can choose the next experiment to be the one that maximizes the utility,

$$e_{n+1} = \operatorname{argmax}_e U_n(e), \quad (5)$$

with the maximum taken over some space of possible experiments. If computed numerically, we might only hope to find local maxima.

One can consider different choices of utility function  $U$ . When the application is inference of a non-linear system, such as ours, it is common to choose a utility based on mean-squared error [1]. In particular, we choose  $U_n = -r_{n,Q}$  where

$$r_{n,Q}(x, d, e) = \operatorname{Tr} [Q(x - \hat{x}_{n,d,e})^T(x - \hat{x}_{n,d,e})] \quad (6)$$

where  $Q$  is a positive semi-definite weighting matrix. Here,  $\hat{x}_{n,d,e} = \int x\tilde{\pi}_{n,d,e}(x)dx$  is the Bayes estimator of  $x$ . In this case,  $r_{n,Q}(e)$  has the simple interpretation of being the expected posterior covariance matrix weighted against  $Q$ ,

$$r_{n,Q}(e) = \operatorname{Tr} [QE_d[\operatorname{Cov}_{\tilde{\pi}}[x|d, e]]], \quad (7)$$

a quantity known as the  $Q$ -weighted mean-squared-error *Bayes risk* (some numerical implementation details are outlined in Section C).

<sup>1</sup> Note that  $\tilde{\pi}_{n,d,e}(x)\Pr(d|e) = \Pr(x, d|x_{1:n}, d_{1:n}, e)$ , and therefore  $U_n(e)$  is the joint average over  $x$  and  $d$  of  $U_n(x, d, e)$  given the current state knowledge—this is a description some may prefer to the two-step description involving the intermediate quantity  $U_n(d, e)$  provided in the main-body.

#### IV. NITROGEN VACANCY SYSTEM MODEL

The quantum system used in our experiment is a nitrogen vacancy (NV) center, which is a defect found in diamond consisting of a nitrogen adjacent to a vacant lattice position [39]. Our goal for this section is to explicitly define model parameters, experiment configurations, and a likelihood function for this system. Once this is achieved, we will be able to employ sequential Bayesian inference and online experiment design.

When in its stable negatively charged configuration,  $\text{NV}^-$ , the vacancy is filled with six electrons that form an effective spin-1 particle in the optical ground state—this three level subspace comprises the system of interest. The eigenstates are labeled  $|1\rangle$ ,  $|0\rangle$ , and  $|-1\rangle$ , respectively corresponding to the eigenvalues of the spin-1 operator  $\mathbf{S}_z = \operatorname{diag}(1, 0, -1)$ . There is a zero field splitting (ZFS) of  $D \approx 2.87$  GHz between  $|0\rangle$  and the span( $|-1\rangle, |+1\rangle$ ) manifold that—at low fields ( $\lesssim 100$  G)—is the dominant energy term, defining our  $z$ -axis. The Zeeman splitting between the states  $|-1\rangle$  and  $|+1\rangle$  is determined by the magnetic field projection onto the  $z$ -axis, equal to  $\omega_e = \gamma_e|B_z|$  in the secular approximation, where  $\gamma_e \approx 2.80$  MHz/G. Spin manipulation is achieved with resonant microwave driving near the transitions  $D \pm \omega_e$ . Long coherence times are observed at room temperature, where the spin state can be initialized and measured optically, and single defects are studied in isolation using confocal microscopy.

In the rotating frame  $\omega_{\mu w}\mathbf{S}_z^2$ , with the rotating wave and secular approximations, the Hamiltonian of the optical ground state is given by

$$H/2\pi = (D - \omega_{\mu w})\mathbf{S}_z^2 + (\omega_e + A\mathbf{I}_z)\mathbf{S}_z + \Omega_1(t)\mathbf{S}_x \quad (8)$$

where  $(\mathbf{S}_x, \mathbf{S}_y, \mathbf{S}_z)$  are the spin-1 operators,  $\omega_{\mu w}$  is the applied microwave frequency,  $\Omega_1(t)$  is the microwave drive strength,  $A$  is the hyperfine splitting due to the adjacent nitrogen-14 atom, and  $\mathbf{I}_z$  is the nitrogen spin-1 operator along  $z$ . Along with the  $T_2^*$  decoherence time that introduces the Lindblad operator  $L = \sqrt{1/T_2^*}\mathbf{S}_z$ , these parameters are sufficient to simulate the experiments that we perform. Therefore, the model parameters of our spin

system (a few more nuisance parameters will be added later) are given by

$$x = (\Omega, \omega_e, \delta D, A, (T_2^*)^{-1}) \quad (9)$$

where  $\delta D = D - 2.87$  GHz. Here,  $\Omega$  is the maximum possible value that  $\Omega_1(t)$  can take, so that we can write  $\Omega_1(t) = a(t)\Omega$  using the unitless pulse-profile function  $a(t) : [0, t_e] \rightarrow [-1, 1]$  of duration  $t_e$ .

A general experiment configuration is then specified by

$$e = (a(t), \omega_{\mu w}, N) \quad (10)$$

where  $a(t)$  pulse profile,  $\omega_{\mu w}$  is the applied microwave frequency, and  $N$  is the number of repetitions of this experiment<sup>2</sup>. In this paper, we restrict our attention to two special cases of this general form, depicted in [Figure 2](#), given by

1. Rabi experiments,  $e_{\text{Rabi}} = (t_p, \omega_{\mu w}, N)$ ,  $a(t) = 1$  for all  $0 \leq t \leq t_e = t_p$ ; and
2. Ramsey experiments,  $e_{\text{Ramsey}} = (t_p, t_w, \omega_{\mu w}, N)$ ,

$$a(t) = \begin{cases} 0 & t_p < t < t_p + t_w \\ 1 & \text{else} \end{cases}$$

for all  $0 \leq t \leq t_e = 2t_p + t_w$ .

Given a hypothetical set of model parameters  $x$  and an experiment configuration  $e$ , the superoperator (in column-stacking convention) is given by the solution to the Lindblad master equation,

$$S(x, e) = \mathcal{T} e^{\int_0^{t_e} (C[H(t)] + D[L]) dt}, \quad \text{where} \quad (11a)$$

$$C[H(t)] = -i(\mathbb{I} \otimes H(t) - \overline{H(t)} \otimes \mathbb{I}) \quad \text{and} \quad (11b)$$

$$D[L] = \overline{L} \otimes L - (\mathbb{I} \otimes L^\dagger L + \overline{L^\dagger L} \otimes \mathbb{I})/2, \quad (11c)$$

and where  $\mathcal{T}$  is Dyson's time ordering operator. This results in the measurement probability

$$p(x, e) = \langle\langle P_0 | S(x, e) | \rho_0 \rangle\rangle, \quad (12)$$

where our initial state is  $\rho_0 = |0\rangle\langle 0| \otimes \mathbb{I}/3$  and the measurement projector is  $P_0 = 3\rho_0$ .

The standard measurement protocol of the NV system at room temperature does not have direct access to strong measurements [\[40\]](#). Instead, the probability  $p(x, e)$  is obstructed by three Poisson rates, so that data is in the form of a triple  $d = (X, Y, Z)$  where

$$X|\alpha \sim \text{Poisson}(N\alpha) \quad (13a)$$

$$Y|\beta \sim \text{Poisson}(N\beta) \quad (13b)$$

$$Z|x, e, \alpha, \beta \sim \text{Poisson}(N(\beta + p(x, e)(\alpha - \beta))) \quad (13c)$$

<sup>2</sup> The experiment configuration must also specify values for each of the timings labeled in [Figure 2](#), but as they are calibrated independently from the experiment of interest, we omit them here for simplicity.

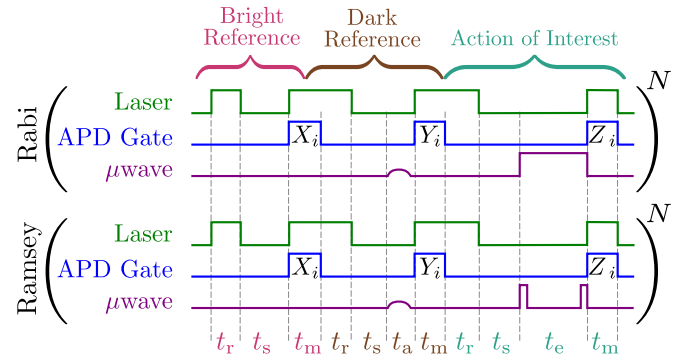


Figure 2: Pulse timing diagrams for Rabi (top) and Ramsey (bottom) experiments. An experiment has three control lines: whether the laser is on or off, whether the APD is counting photons or not, and the microwave amplitude profile. The pulse sequence is repeated  $N$  times, collecting photon counts ( $X_i, Y_i, Z_i$ ) for  $i = 1, \dots, N$  for the bright reference, dark reference, and experiment, respectively, and finally summing them each over  $i$  to produce the data point  $d = (X, Y, Z)$ . Initial states are prepared by lasing for time  $t_r$  and letting the system settle for time  $t_s$ . Measurements consist of detecting photons for durations of length  $t_m$  while lasing. The dark reference includes an adiabatic pulse of length  $t_a$  which causes the state transfer  $|0\rangle \rightarrow |+1\rangle$ . The action of interest implements the microwave envelope  $\Omega_1(t)$  of duration  $t_e$ . Relative timing is not to scale in this diagram.

with  $\alpha$  and  $\beta$ , the number of expected photons for the bright and dark references in a single shot with a given measurement duration  $t_m$ , satisfying  $0 < \beta < \alpha$ . The values  $\alpha$  and  $\beta$  are nuisance parameters which we must append to our model parameters, giving

$$x = (\Omega, \omega_e, \delta D, A, (T_2^*)^{-1}, \alpha, \beta). \quad (14)$$

The likelihood function (see [Equation 1](#)) for a single experiment is then given by

$$\begin{aligned} L(x; d, e) &= f(X, N\alpha) \cdot f(Y, N\beta) \\ &\quad \times f(Z, N(\beta + p(x, e)(\alpha - \beta))) \end{aligned} \quad (15)$$

where  $f$  is the probability mass function of the Poisson distribution,  $f(Q, \lambda) = e^{-\lambda} \lambda^Q / Q!$ . Some example risk plots ([Equation 7](#)) of this model are shown in [Figure 3](#).

## V. COMPUTATION AND HARDWARE

For all experiment design heuristics, offline and online, we use the sequential Monte Carlo (SMC) [\[41\]](#) method to numerically compute sequential posteriors using the Python library QInfer[\[42\]](#). In this algorithm, the state of knowledge about the model parameters,  $\pi_n(x)$ , is approximated as a finite list of weighted hypothetical values (which are called *particles*),

$$\pi_n(x) = \sum_{i=1}^K w_{n,i} \delta(x - x_{n,i}), \quad (16)$$

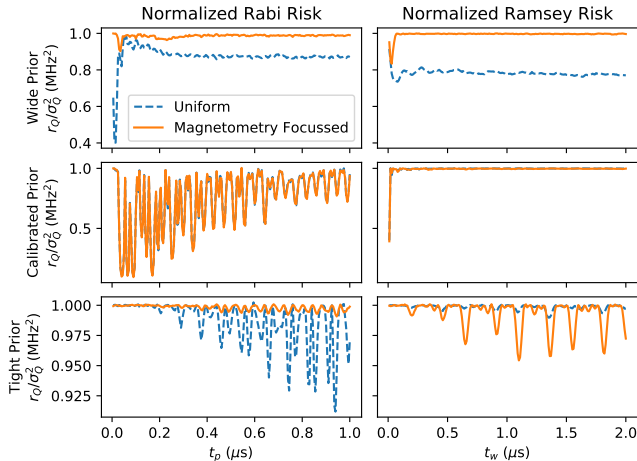


Figure 3: Calculation of risk for three different prior distributions (rows) and for both Rabi and Ramsey type experiments (columns). The dashed blue lines use a uniform weight matrix  $Q = \text{diag}(1, 1, 1, 1, 1)$ , and the solid orange lines use a weight matrix focused only on  $\omega_e$ ,  $Q = \text{diag}(0, 1, 0, 0, 0)$ . Values have been normalized against  $\sigma_Q^2 = \text{Tr}(Q \text{Cov}_\pi[x])$  where  $\text{Cov}_\pi[x]$  is the covariance matrix of a prior distribution  $\pi$ , so that, for example, a value of  $r_Q(e)/\sigma_Q^2 = 0.95$  for a given experiment  $e$  implies a 5% expected improvement in weighted covariance. The wide prior (top row) is defined in Equation 20, the calibrated prior (middle row) is defined in Equation 21, and the tight prior (bottom row) is the same as the calibrated prior, but without widening the  $\omega_e$  parameter. Note that the Rabi and Ramsey experiments share a  $y$ -axis on each row. We see that, among these examples, the only beneficial setting to perform a Ramsey experiment is with the tight prior when  $\omega_e$  is the parameter of interest.

where  $w_{n,i} \geq 0$  with  $\sum_{i=1}^K w_{n,i} = 1$ , and where  $\delta(\cdot)$  is the delta mass distribution centered at 0. The particle-approximated prior,  $\pi_0(x)$ , is generated by sampling  $K$  initial particles  $x_{0,i}$  from the prior distribution and setting uniform weights  $w_{0,i} = 1/K$ . Given the new datum  $d_{n+1}$  under experiment configuration  $e_{n+1}$ , Bayes update can be implemented with the simple multiplication

$$w_{n+1,i} \propto w_{n,i} \cdot L(x_{n,i}; d_{n+1}, e_{n+1}) \quad (17)$$

which requires  $K$  simulations of the quantum system to compute the likelihoods (Equation 15), and where the constant of proportionality is chosen so that  $\sum_{i=1}^K w_{n+1,i} = 1$ . We use the scheme of Liu and West [43] to resample particle locations, triggered by a threshold in the effective particle count,  $n_{\text{eff}} := 1/\sum_{i=1}^K w_{n,i}^2$  [42]. We also use the bridged-updating trick discussed in Reference [40].

We note that the expensive stage of this algorithm is embarrassingly parallel—simulations under the various model parameters  $x_{n,i}$  can be performed independently. All of our processing was run on a desktop computer with simulations parallelized over the 12 cores on a pair of Intel Xeon X5675 CPUs. In this configuration, our updates took on the order of 2 seconds with  $K = 30000$

particles. In principle, simulations could instead be run on quantum simulators, as was recently demonstrated [44].

For online heuristics, the Bayes risk (Equation 7) is calculated by noting that the particle approximation turns all integrals, which includes expectations and covariances, into finite sums—see Section C for details. Some risk calculations for the NV model are plotted in Figure 3. As seen in the timing diagram in Figure 1, these calculations (along with the Bayes updates) are performed concurrently with experiments so that they do not add to experiment cost<sup>3</sup>. This causes the side-effect where the next experiment is selected using information that is one cycle out-of-date; however, in our simulations at our data collection rates, we found that this did not have a noticeable effect on learning rates. A new experiment configuration  $e_{n+1}$  having been decided, by whatever heuristic, the processing computer sends  $e_{n+1}$  to the computer which controls experiments. The experiment is run, and the datum  $d_{n+1} = (X, Y, Z)$  is returned to the processing computer. This process is iterated until some stopping criterion is met—for example, in our experiments, we chose to stop after 200 experiments had been performed.

In our setup, the processing computer and the experiment computer communicate over ethernet with TCP. We use a custom built confocal microscope to isolate an individual NV center in bulk diamond. All of our experiments were performed on the same NV center. Laser light is produced by a continuous-wave 100 mW laser at 532 nm, and switched using a double pass through an acousto-optic modulator. Photons are collected with an avalanche-photo detector (APD). Microwaves are transmitted to the NV by an antenna of diameter 25  $\mu\text{m}$  about 100  $\mu\text{m}$  away from the defect, generated by a microwave synthesizer, and shaped by two channels of an arbitrary waveform generator (AWG) that mix via an IQ modulation. Experimental configurations are manifest as waveforms on the AWG. We use a caching strategy, where the experiment computer uses a hash table to check if the desired experiment already exists in the AWGs memory, avoiding data transfer costs when possible.

## VI. EFFECTIVE STRONG MEASUREMENTS AND DRIFT TRACKING

The amount of information provided by a measurement of  $Z$  (see Equation 13) depends on the values of  $\alpha$  and  $\beta$ . Their magnitudes, relative contrast, and uncertainty all contribute to this information content. We quantify this idea by introducing what we call the number of *effective strong measurements* (ESM), defined as the number of

<sup>3</sup> Of course, this is only possible so long as the experiment repetition count is large enough compared to the parallelized simulation cost. In our setup, at our count rates, we landed naturally in this regime with CPU computation a single desktop computer.

two-outcome strong measurements one would (hypothetically) have to do to gain the equivalent amount of information about  $p(x, e)$ , averaged uniformly over  $p \in [0, 1]$ . This works out to

$$\text{ESM} = \frac{(\hat{\alpha} - \hat{\beta})^2}{3(\hat{\alpha} + \hat{\beta}) + 2(\sigma_\alpha^2 + \sigma_\beta^2)}. \quad (18)$$

where  $\hat{\alpha}$  and  $\hat{\beta}$  are our current estimates of  $\alpha$  and  $\beta$ , and  $\sigma_\alpha$  and  $\sigma_\beta$  are standard deviation uncertainties in these estimates. See Section B for details. We choose the number of repetitions in the next experiment,  $N$ , such that the expected value of ESM is constant—see Figure 4(b-c). This is especially important for the purpose of our paper, which is to compare experiment design heuristics. In this way, certain heuristics are not artificially improved because of favorable lab conditions on a certain day of the week.

The true specific values of the references  $\alpha$  and  $\beta$  depend not only on the optical dynamics of the quantum system itself, but also on the quality of the microscope’s alignment. As the temperature of the lab changes, for instance, one can expect the values of  $\alpha$  and  $\beta$  to drift as the location of the NV center moves with respect to the focal spot of the microscope. To account for this, a tracking operation is performed periodically, where the focus of microscope is repositioned based on a new set of images taken with the microscope.

A model that assumes these reference values are constant in time can lead to inaccurate results, or even failure. To account for this drift, we append a Gaussian random walk model for the parameters  $\alpha$  and  $\beta$  to the static model defined in Section IV. Specifically, we assume that immediately prior to a particle update (Equation 17) the reference indices of the each model parameter particle undergo a resampling step defined as

$$\begin{pmatrix} \alpha_{n,i} \\ \beta_{n,i} \end{pmatrix} \sim \text{Normal} \left( \begin{pmatrix} \alpha_{n,i} \\ \beta_{n,i} \end{pmatrix}, \Delta t \begin{pmatrix} \sigma_\alpha^2 & \sigma_{\alpha,\beta} \\ \sigma_{\alpha,\beta} & \sigma_\beta^2 \end{pmatrix} \right), \quad (19)$$

where  $\Delta t$  is the amount of time elapsed since the last update. The hyper-parameters  $\sigma_\alpha$ ,  $\sigma_\beta$ , and  $\sigma_{\alpha,\beta}$  are treated as unknown; they are appended to the model parameters, and co-learned along with the parameters defined in Equation 14. We use a wide inverse Wishart distribution as the prior with a degrees-of-freedom parameter  $\nu = 30$  and a scale matrix  $\Psi$  such that the mean value of the prior corresponds to  $\sigma_\alpha = \sigma_\beta = \sigma_{\alpha,\beta}/0.7 = 0.036$  /hour. We use an empirical prior on  $\alpha$  and  $\beta$ , where before the actual experiments take place, a reference-only experiment is performed with  $N = 300000$  repetitions, and the prior is set as  $\alpha \sim \text{Gamma}(\mu = X/N, \sigma = 3\sqrt{X}/N)$  and  $\beta \sim \text{Gamma}(\mu = Y/N, \sigma = 3\sqrt{Y}/N)$ . When a tracking operation is performed, the distribution of  $\alpha$  and  $\beta$  is resampled from the prior  $\pi_0(x)$ , with all other parameters of the model held fixed. We chose to perform tracking operation at the start of each trial, and each time our estimate of  $\alpha$  dipped below our prior estimate of  $\alpha$  minus five times the standard deviation of our prior for  $\alpha$ .

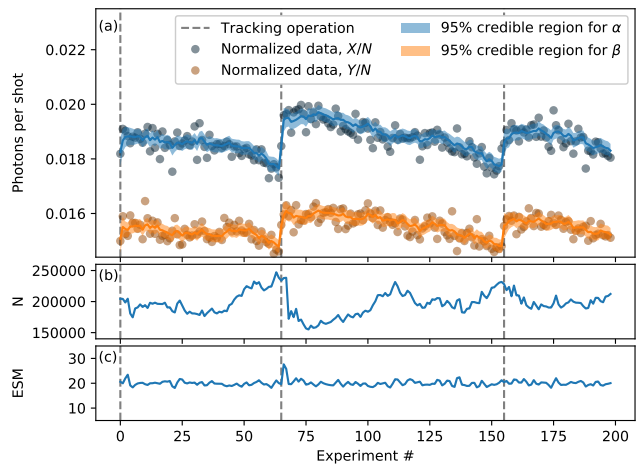


Figure 4: An NV drift tracking example, where tracking operations take place at the vertical dashed lines. (a) Subpoissonian 95% credible regions are shown on top of data normalized by the experiment repetition count,  $N$ . (b) The repetition count was chosen online to maintain a constant ESM value of 20, which is plotted in (c). Several hundred trials were searched through to find this extreme but illustrative example—references are typically quite flat.

## VII. RESULTS

There are many choices to be made, even for this small system. For example, we have already limited ourselves to Rabi and Ramsey experiments. Put differently, and given that our free evolution commutes with both our initial state and measurement, we have limited ourselves to bang-bang control with a maximum of two pulses. This is to ease simulations (bang-bang), and to reduce the search space for online heuristics (two pulses or fewer). We simplify the situation further by choosing to work in the low field regime, say  $\lesssim 3$  G. This saves us from having to adaptively modify the synthesizer frequency  $\omega_{\mu w}$ ; we keep a fixed value of  $\omega_{\mu w} = 2.87$  GHz for all experiments. It also prevents us from having to make decisions about the relative phase between the two Ramsey pulses, to which we are almost entirely insensitive at low field and with linearly polarized microwaves. These particular choices are by no means necessary, but serve as a starting place to explore the landscape. From the perspective of metrology, these choices amount to studying the efficiency of DC magnetometry at low field with the NV system using the double quantum manifold.

In our first comparison between experiment design heuristics, we use a wide prior on the Hamiltonian pa-

Heuristic	Definition
Alternating Linear	Offline; Sequential alternation between elements of the experiment sets $E_{\text{Rabi}}(500 \text{ ns}, 100)$ and $E_{\text{Ramsey}}(\hat{t}_{\text{p,best}}, 2 \text{ us}, 100)$
Ramsey Sweeps	Offline; Two back-to-back sweeps through the experiment set $E_{\text{Ramsey}}(\hat{t}_{\text{p,best}}, 2 \text{ us}, 100)$
Uniformly Weighted Risk	Online; $e_{n+1} = \operatorname{argmax}_{e \in E} (r_{n,Q}(e))$ where $Q = \operatorname{diag}(1, 1, 1, 1, 1)$ and $E = E_{\text{Rabi}}(500 \text{ ns}, 100) \cup E_{\text{Ramsey}}(\hat{t}_{\text{p,best}}, 2 \text{ us}, 100)$
Magnetometry Weighted Risk	Online; $e_{n+1} = \operatorname{argmax}_{e \in E} (r_{n,Q}(e))$ where $Q = \operatorname{diag}(0, 1, 0, 0, 0)$ and $E = E_{\text{Rabi}}(500 \text{ ns}, 100) \cup E_{\text{Ramsey}}(\hat{t}_{\text{p,best}}, 2 \text{ us}, 100)$

Table I: Summary of heuristics used to choose experiments. The best Ramsey tip time is defined by  $\hat{t}_{\text{p,best}} = 1/(4\hat{\Omega})$  (rounded to the nearest 2 ns), where  $\hat{\Omega}$  is the current Bayes estimate of the microwave drive amplitude.  $E_{\text{Rabi}}(t_{\text{max}}, m)$  denotes a set of Rabi experiments with pulse times  $t_{\text{p}} = t_{\text{max}}/m, 2t_{\text{max}}/m, \dots, t_{\text{max}}$ , and  $E_{\text{Ramsey}}(t_{\text{p}}, t_{\text{max}}, m)$  denotes a set of Ramsey experiments with wait times  $t_{\text{w}} = t_{\text{max}}/m, 2t_{\text{max}}/m, \dots, t_{\text{max}}$  and pulse times  $t_{\text{p}}$ . The components of weight matrices  $Q$  correspond to the Hamiltonian parameters  $(\Omega, \omega_e, \delta D, A, (T_2^*)^{-1})$ , with zeros for reference parameters.

rameters given by

$$\Omega/\text{MHz} \sim \text{Unif}([0, 20]), \quad (20\text{a})$$

$$\omega_e/\text{MHz} \sim \text{Unif}([0, 10]), \quad (20\text{b})$$

$$\delta D/\text{MHz} \sim \text{Unif}([-5, 5]), \quad (20\text{c})$$

$$A/\text{MHz} \sim \text{Unif}([1.5, 3.5]), \quad (20\text{d})$$

$$T_2^*/\mu\text{s} \sim \text{Unif}([1, 20]). \quad (20\text{e})$$

along with the reference priors discussed in [Section VI](#). We implement the offline heuristic *Alternating Linear* and the online heuristics *Uniformly Weighted Risk* and *Magnetometry Weighted Risk* defined in [Table I](#). The offline heuristic is motivated by standard DC magnetometry, where, intuitively, Rabi experiments are used to determine the pulse length that causes  $|0\rangle \mapsto \frac{|+1\rangle + |-1\rangle}{\sqrt{2}}$ , and Ramsey experiments subsequently exploit this superposition state to measure the relative phase accumulation between  $|+1\rangle$  and  $|-1\rangle$ , which is proportional to  $t_{\text{w}}\omega_e$ . Note that, unconventionally, this heuristic alternates between Rabi and Ramsey experiments, as was done in [\[40\]](#)—this improves numerical stability of the SMC sampler; as different experiments are statistically independent, alternation does not affect the overall information content. The two online experiments differ only in the weighting matrix  $Q$  that is used—the first weights all quantum system parameters equally, and the second projects risk onto only one parameter,  $\omega_e$ .

Results of this first comparison are shown in [Figure 5\(a-c\)](#). Here, it is seen that both online heuristics outperform the offline heuristic, with a final gap of a bit more than two orders of magnitude in the median (over trials) posterior variance of  $\omega_e$  after 4000 ESM. In the histograms we see that the magnetometry focused online heuristic uses almost all Ramsey experiments, and the uniformly weighted online heuristics uses almost all Rabi experiments, which agrees with the risk profiles plotted in [Figure 3](#). We see also that the offline heuristic has a much larger spread in posterior variances across trials (area of shaded regions), where some trials perform almost as well

as the online heuristics, but many perform significantly worse. In this sense, in addition to tighter posteriors on average, these online heuristics have the extra advantage of being more reliable. Our guess is that offline heuristics require luckily informative data at certain key experiments to perform well, whereas online experiments can simply repeat these key experiments. Finally, note that the magnetometry focused online heuristic slightly outperforms the evenly weighted online heuristic—this is unsurprising as we happen to be plotting the variance of the magnetometry parameter,  $\omega_e$ .

In the context of magnetometry, it is unrealistic to assume such a wide prior as given in [Equation 20](#). More likely, one has already calibrated the quantum device and wants to learn only the value of  $\omega_e$ . For example, one might be constructing a magnetic image [\[45–47\]](#), and each pixel of the image requires a new field measurement. Therefore, for our second comparison, we place a prior that is tight in all Hamiltonian parameters except  $\omega_e$ , given as

$$\omega_e/\text{MHz} \sim \text{Unif}([0, 10]), \quad (21\text{a})$$

$$(\Omega, \delta D, A, (T_2^*)^{-1})/\text{MHz} \sim \text{Normal}(\mu_{\text{cal}}, \Sigma_{\text{cal}}), \quad (21\text{b})$$

where  $\mu_{\text{cal}}$  and  $\Sigma_{\text{cal}}$  are taken

from the posterior of a set of previously run calibration experiments, see [Section A](#) for details. In our study of this second prior, in addition to the three heuristics used above, we consider another heuristic called *Ramsey Sweeps* that uses only Ramsey experiments, since they are the *de facto* method for measuring static Hamiltonian terms along  $z$ . Results for this second prior are shown in [Figure 5\(d-f\)](#). There are a few interesting features. The first is that it is clearly visible where the *Ramsey Sweeps* heuristic finishes one sweep and starts the next, at 2000 ESM. The second is that all three of the heuristics that were also used for the wide prior ([Equation 20](#)) have significantly less spread under the calibrated prior. The third is that the magnetometry weighted online heuristic has a much clearer advantage

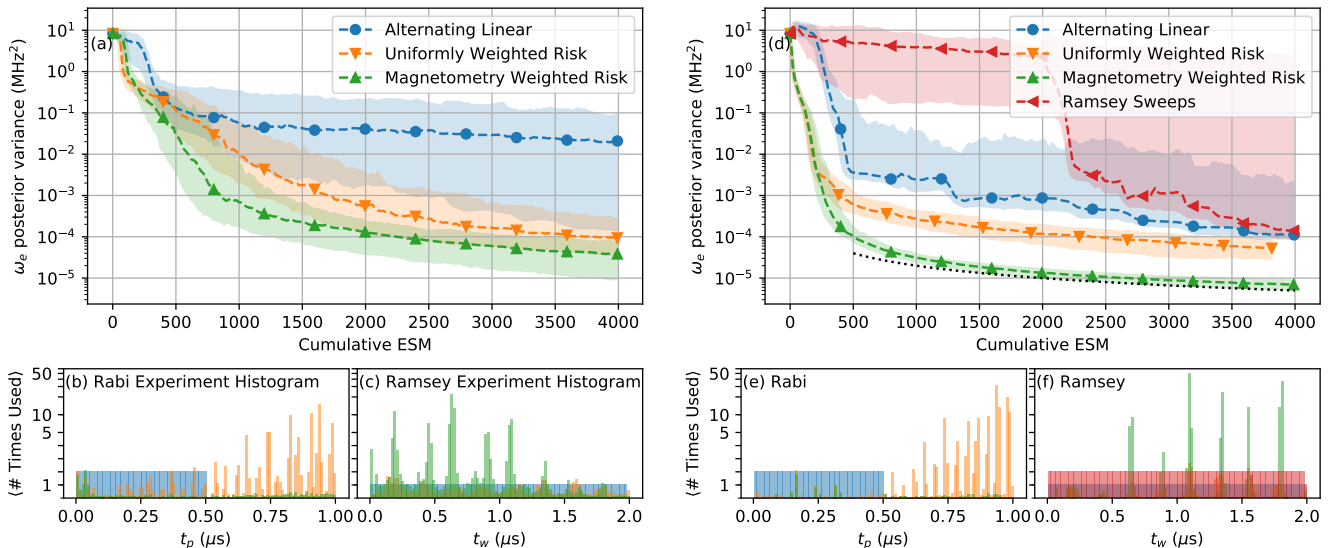


Figure 5: Comparison of experiment design heuristics (see Table I) where each heuristic was run with 100 independent trials using 200 experiments per trial. The left figures (a-c) use the wide prior of Equation 20, and the right figures (d-f) use the calibrated prior of Equation 21. (a,d) For the parameter  $\omega_e$ , the median posterior variance over 100 trials is plotted (dashed lines), and regions between the 10% and 90% percentiles are shaded. The  $x$ -axes display ESM (effective strong measurements), where roughly 20 effective bits of data are collected per experiment, see Section VI. The black dotted line scales as  $\text{ESM}^{-1}$ . In (b-c,e-f), histograms of which experiments each heuristic uses are shown, normalized to represent the average number of times used per trial. Note that the  $y$ -axis between histograms is shared, that the scaling switches from linear to logarithmic at  $y = 5$ , and that all four subfigures contain 100 histogram bins. Additional learning curves are plotted in Section A.

over the uniformly weighted online heuristic than in the case of the wide prior comparison. Finally, notice in the histograms, that the uniformly weighted online heuristic again chooses Rabi experiments almost exclusively.

Supplementary plots, including posterior distributions, can be found in Section A.

Our online learning rates appear to be at the standard quantum limit (SQL) once transient behavior has settled down; the dotted line in Figure 5(d) guides the eye with a curve  $\propto \text{ESM}^{-1}$ . The transient behavior prior to the SQL regime looks qualitatively exponential as a function of ESM. This does not violate the Heisenberg limit ( $\sigma^2 \propto \text{ESM}^{-2}$ ) because experiment times,  $t_e$ , are able to exponentially increase, too [23]. Exponential-into-SQL scaling is consistent with previous Hamiltonian estimation research, where the coherence time of the system controls the transition location—ideally we would perform Ramsey experiments with arbitrarily long wait times, but finite  $T_2^*$  makes such experiments uninformative [25].

## VIII. CONCLUSIONS

We compared the ability of several experiment design heuristics to experimentally learn the electronic ground state Hamiltonian of an NV defect in diamond. Some of our heuristics were offline—using experiment sweeps that were predetermined, and some of heuristics were online—

using knowledge gained from previous experiments to choose the next experiment adaptively. The heuristics we used are summarized in Table I. All data analysis was done with sequential Bayesian inference, and all online heuristics were based on minimizing the weighted Bayes risk over a collection of possible experiments. Heuristics were compared by running 100 independent trials of each, and comparing the reduction in posterior variance of certain parameters as a function of the number of experiments performed.

We found that our online heuristics outperformed our offline heuristics; results are summarized in Figure 3. In particular, in the case of a very wide prior on all parameters (Figure 5(a-c)), we found that the median posterior variance of the parameter  $\omega_e$ —which is proportional to the external magnetic field’s projection onto the  $z$ -axis—is over two orders of magnitude smaller after 200 experiments (comprising 200 effective strong measurements per experiment) for the online heuristic called *Magnetometry Weighted Risk* than it is for the offline heuristic called *Alternating Linear*. Next, in the case of a prior that is tight on all parameters except  $\omega_e$  (Figure 5(d-f)), we found about an order of magnitude of improvement between the best online heuristic and the best offline heuristic. The use case of this prior is when one wants to use a calibrated NV device to measure many magnetic fields.

Consistent with intuition, we found that when online experiments are weighted to improve  $\omega_e$  alone, they tend to choose Ramsey experiments almost exclusively, rather

than Rabi experiments, see [Figure 5\(b-c,e-f\)](#).

In addition to faster decrease in variance, we also found that variance decreases more predictably for online heuristics than it does for predetermined heuristics. This is seen in the tighter 80% percentile regions of [Figure 5\(a,d\)](#) for online experiments. For example, the difference in the final posterior variance of the parameter  $\omega_e$  varies by as much as four orders of magnitude between independent trials for the *Ramsey Sweeps* heuristic, whereas it always varies by less than one order of magnitude for all online heuristics.

Studies of the sort presented here necessarily suffer from having to make choices—in the end we had to choose a small number of heuristics to compare, which types of experiments heuristics should be allowed to perform, what the hyper-parameters of each heuristic should be, what the initial prior over parameters should be, and so on. Though these choices are ultimately arbitrary, we attempted to make them reasonable, with the end goal of comparing a fully brute-force Bayesian scheme against what have historically been the *de facto* methods of characterization. While we would not be surprised to find a

less computationally expensive experiment design heuristic for this particular problem with similar performance (for example, see the heuristic policies in [\[28\]](#)), the advantage of a full-risk based approach is that it doesn't require an expert to design a heuristic for every particular combination system and protocol. Indeed, minimizing Bayes risk, if computationally feasible either with classical or quantum resources, is a sensible approach for practically any characterization protocol, from tomography to randomized benchmarking.

### Acknowledgments

The authors gratefully acknowledge contributions from the Canada First Research Excellence Fund, Industry Canada, Canadian Excellence Research Chairs, the Natural Sciences and Engineering Research Council of Canada, the Canadian Institute for Advanced Research, and the Province of Ontario.

- 
- [1] K. Chaloner and I. Verdinelli, [Statistical Science](#) **10**, 273 (1995).
  - [2] B. L. Higgins, D. W. Berry, S. D. Bartlett, M. W. Mitchell, H. M. Wiseman, and G. J. Pryde, [New Journal of Physics](#) **11**, 073023 (2009).
  - [3] R. Freeman, H. D. W. Hill, and R. Kaptein, [Journal of Magnetic Resonance](#) (1969) **7**, 82 (1972).
  - [4] H. Taitelbaum, J. A. Ferretti, R. G. S. Spencer, and G. H. Weiss, [Journal of Magnetic Resonance, Series A](#) **105**, 59 (1993).
  - [5] H. M. Wiseman, [Physical Review Letters](#) **75**, 4587 (1995).
  - [6] D. W. Berry, H. M. Wiseman, and J. K. Breslin, [Physical Review A](#) **63**, 053804 (2001).
  - [7] B. L. Higgins, D. W. Berry, S. D. Bartlett, H. M. Wiseman, and G. J. Pryde, [Nature](#) **450**, 393 (2007).
  - [8] D. W. Berry, B. L. Higgins, S. D. Bartlett, M. W. Mitchell, G. J. Pryde, and H. M. Wiseman, [Physical Review A](#) **80**, 052114 (2009).
  - [9] G. Y. Xiang, B. L. Higgins, D. W. Berry, H. M. Wiseman, and G. J. Pryde, [Nature Photonics](#) **5**, 43 (2011).
  - [10] H. Yonezawa, D. Nakane, T. A. Wheatley, K. Iwasawa, S. Takeda, H. Arao, K. Ohki, K. Tsumura, D. W. Berry, T. C. Ralph, H. M. Wiseman, E. H. Huntington, and A. Furusawa, [Science](#) **337**, 1514 (2012).
  - [11] M. A. Ciampini, N. Spagnolo, C. Vitelli, L. Pezzè, A. Smerzi, and F. Sciarrino, [Scientific Reports](#) **6**, 28881 (2016).
  - [12] F. Huszár and N. M. T. Houlby, [Physical Review A](#) **85**, 052120 (2012).
  - [13] K. S. Kravtsov, S. S. Straupe, I. V. Radchenko, N. M. T. Houlby, F. Huszár, and S. P. Kulik, [Physical Review A](#) **87**, 062122 (2013).
  - [14] C. Ferrie, [Physical Review Letters](#) **113**, 190404 (2014).
  - [15] M. P. V. Stenberg, K. Pack, and F. K. Wilhelm, [Physical Review A](#) **92**, 063852 (2015).
  - [16] G. I. Struchalin, I. A. Pogorelov, S. S. Straupe, K. S. Kravtsov, I. V. Radchenko, and S. P. Kulik, [Physical Review A](#) **93**, 012103 (2016).
  - [17] C. Granade, J. Combes, and D. G. Cory, [New Journal of Physics](#) **18**, 033024 (2016).
  - [18] B. Qi, Z. Hou, Y. Wang, D. Dong, H.-S. Zhong, L. Li, G.-Y. Xiang, H. M. Wiseman, C.-F. Li, and G.-C. Guo, [npj Quantum Information](#) **3**, 19 (2017).
  - [19] C. Granade, C. Ferrie, and D. G. Cory, [New Journal of Physics](#) **17**, 013042 (2015).
  - [20] D. J. Egger and F. K. Wilhelm, [Physical Review Letters](#) **112**, 240503 (2014).
  - [21] C. Ferrie and O. Moussa, [Physical Review A](#) **91**, 052306 (2015).
  - [22] M. A. Rol, C. C. Bultink, T. E. O'Brien, S. R. de Jong, L. S. Theis, X. Fu, F. Luthi, R. F. L. Vermeulen, J. C. de Sterke, A. Bruno, D. Deurloo, R. N. Schouten, F. K. Wilhelm, and L. DiCarlo, [Physical Review Applied](#) **7**, 041001 (2017).
  - [23] A. Sergeevich, A. Chandran, J. Combes, S. D. Bartlett, and H. M. Wiseman, [Physical Review A](#) **84**, 052315 (2011).
  - [24] C. E. Granade, C. Ferrie, N. Wiebe, and D. G. Cory, [New Journal of Physics](#) **14**, 103013 (2012).
  - [25] C. Ferrie, C. E. Granade, and D. G. Cory, [Quantum Information Processing](#) **12**, 611 (2013).
  - [26] N. Wiebe, C. Granade, C. Ferrie, and D. G. Cory, [Physical Review Letters](#) **112**, 190501 (2014).
  - [27] M. P. V. Stenberg and F. K. Wilhelm, [Physical Review A](#) **94**, 052119 (2016).
  - [28] M. P. V. Stenberg, O. Köhn, and F. K. Wilhelm, [Physical Review A](#) **93**, 012122 (2016).
  - [29] A. Gruber, A. Dräbenstedt, C. Tietz, L. Fleury, J. Wrachtrup, and C. von Borczyskowski, [Science](#) **276**,

- 2012 (1997).
- [30] F. Jelezko and J. Wrachtrup, *Journal of Physics: Condensed Matter* **16**, R1089 (2004).
- [31] J. Harrison, M. J. Sellars, and N. B. Manson, *Journal of Luminescence Proceedings of the 8th International Meeting on Hole Burning, Single Molecule, and Related Spectroscopies: Science and Applications*, **107**, 245 (2004).
- [32] F. Jelezko, T. Gaebel, I. Popa, M. Domhan, A. Gruber, and J. Wrachtrup, *Physical Review Letters* **93**, 130501 (2004).
- [33] G. Balasubramanian, P. Neumann, D. Twitchen, M. Markham, R. Kolesov, N. Mizuochi, J. Isoya, J. Achard, J. Beck, J. Tissler, V. Jacques, P. R. Hemmer, F. Jelezko, and J. Wrachtrup, *Nature Materials* **8**, 383 (2009).
- [34] F. Dolde, H. Fedder, M. W. Doherty, T. Nöbauer, F. Rempp, G. Balasubramanian, T. Wolf, F. Reinhard, L. C. L. Hollenberg, F. Jelezko, and J. Wrachtrup, *Nature Physics* **7**, 459 (2011).
- [35] V. M. Acosta, E. Bauch, M. P. Ledbetter, A. Waxman, L.-S. Bouchard, and D. Budker, *Physical Review Letters* **104**, 070801 (2010).
- [36] L. Rondin, J.-P. Tetienne, T. Hingant, J.-F. Roch, P. Maletinsky, and V. Jacques, *Reports on Progress in Physics* **77**, 056503 (2014).
- [37] L. Childress, J. M. Taylor, A. S. Sørensen, and M. D. Lukin, *Physical Review Letters* **96**, 070504 (2006).
- [38] I. Hincks, T. Alexander, M. Kononenko, B. Soloway, and D. Cory, “<https://github.com/ihincks/nv-adaptive>,” (2018).
- [39] M. W. Doherty, N. B. Manson, P. Delaney, F. Jelezko, J. Wrachtrup, and L. C. L. Hollenberg, *Physics Reports The nitrogen-vacancy colour centre in diamond*, **528**, 1 (2013).
- [40] I. Hincks, C. Granade, and D. G. Cory, *New Journal of Physics* **20**, 013022 (2018).
- [41] A. Doucet and A. M. Johansen, *Handbook of nonlinear filtering* **12**, 3 (2009).
- [42] C. Granade, C. Ferrie, I. Hincks, S. Casagrande, T. Alexander, J. Gross, M. Kononenko, and Y. Sanders, *Quantum* **1**, 5 (2017).
- [43] J. Liu and M. West, in *Sequential Monte Carlo Methods in Practice* (Springer, 2001) pp. 197–223.
- [44] J. Wang, S. Paesani, R. Santagati, S. Knauer, A. A. Gentile, N. Wiebe, M. Petruzzella, J. L. O’Brien, J. G. Rarity, A. Laing, and M. G. Thompson, *Nature Physics* **13**, 551 (2017).
- [45] P. Maletinsky, S. Hong, M. S. Grinolds, B. Hausmann, M. D. Lukin, R. L. Walsworth, M. Loncar, and A. Yacoby, *Nature Nanotechnology* **7**, 320 (2012).
- [46] M. S. Grinolds, S. Hong, P. Maletinsky, L. Luan, M. D. Lukin, R. L. Walsworth, and A. Yacoby, *Nature Physics* **9**, 215 (2013).
- [47] L. Rondin, J.-P. Tetienne, S. Rohart, A. Thiaville, T. Hingant, P. Spinicelli, J.-F. Roch, and V. Jacques, *Nature Communications* **4**, 2279 (2013).
- [48] C. W. Ueberhuber, *Numerical Computation 2: Methods, Software, and Analysis* (Springer-Verlag, Berlin Heidelberg, 1997).

## Appendix A: Supplementary Plots and Data

The calibration prior of Equation 21 was generated by processing two trials of the Alternating Linear heuristic, for a total of 400 experiments, and roughly 8000 ESM. The first two moments of the posterior distribution were computed, resulting in the values

$$\mu_{\text{cal}} = \begin{pmatrix} 11.55 \\ -0.86 \\ 2.18 \\ 0.35 \end{pmatrix} \text{MHz} \quad (\text{A1a})$$

$$\Sigma_{\text{cal}} = \begin{pmatrix} 2.56 \times 10^{-5} & 1.02 \times 10^{-3} & 7.67 \times 10^{-7} & 3.80 \times 10^{-5} \\ 1.02 \times 10^{-3} & 1.06 \times 10^{-1} & 1.97 \times 10^{-4} & 2.50 \times 10^{-3} \\ 7.67 \times 10^{-7} & 1.97 \times 10^{-4} & 7.51 \times 10^{-5} & -1.02 \times 10^{-4} \\ 3.80 \times 10^{-5} & 2.50 \times 10^{-3} & -1.02 \times 10^{-4} & 1.01 \times 10^{-3} \end{pmatrix} \text{MHz}^2 \quad (\text{A1b})$$

for the ordered parameters  $(\Omega, \delta D, A, (T_2^*)^{-1})$ , where  $\omega_e$  and nuisance parameters ham been marginalized over.

In Figure 5, only the learning rates of  $\omega_e$  are reported—in Figure 6 and Figure 7, all learning rates are shown. Posteriors are shown in Figure 8 and Figure 9, where the first trial from each heuristic is used as a representative.

## Appendix B: Effective Strong Measurements

Given a quantum state  $\rho$ , information is accessed through the Born’s probability  $p = \text{Tr}(|0\rangle\langle 0|\rho)$ . In the hypothetical case of strong measurement, in the language of statistics, we would be able to draw from the Bernoulli distribution  $\text{Bern}(p)$ , or more generally, with  $n$  repeated preparations and strong measurements, from the binomial distribution  $\text{Binom}(n, p)$ .

Standard room temperature NV setups do not allow strong measurements. Instead, access to the quantity  $p$  is obstructed by three Poisson rates, such that conditional on some values  $0 < \beta < \alpha$ , we can draw from the random

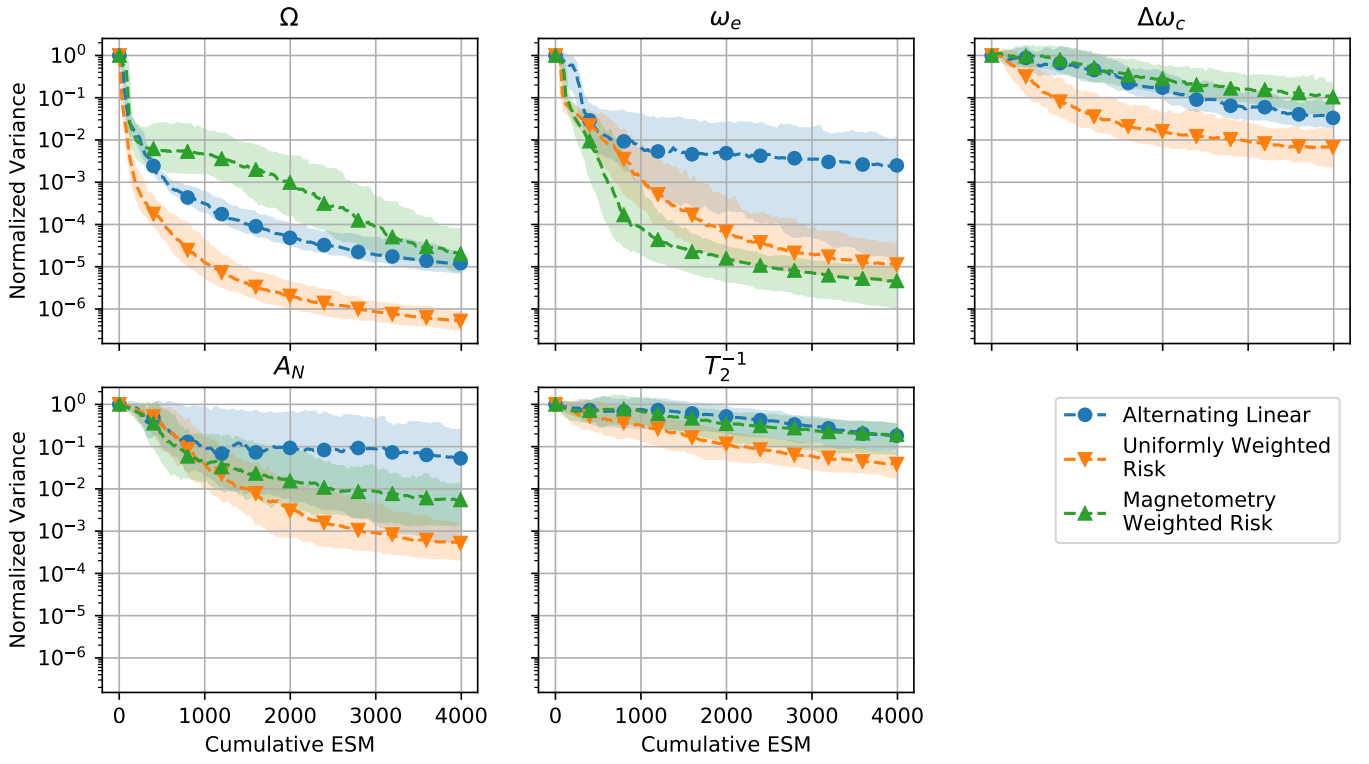


Figure 6: An extension of Figure 5(a-c) that shows learning rates of all parameters relevant to the quantum dynamics of the system.

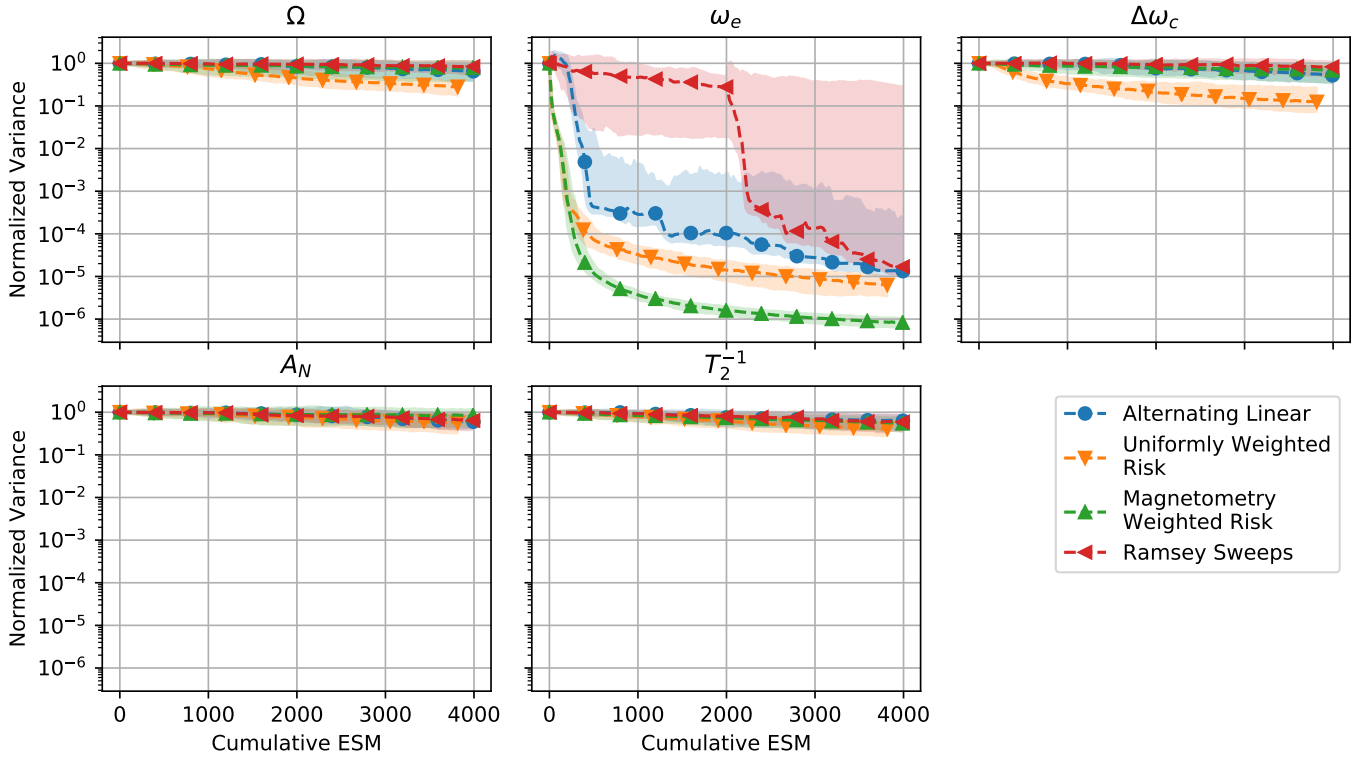


Figure 7: An extension of Figure 5(d-f) that shows learning rates of all parameters relevant to the quantum dynamics of the system.

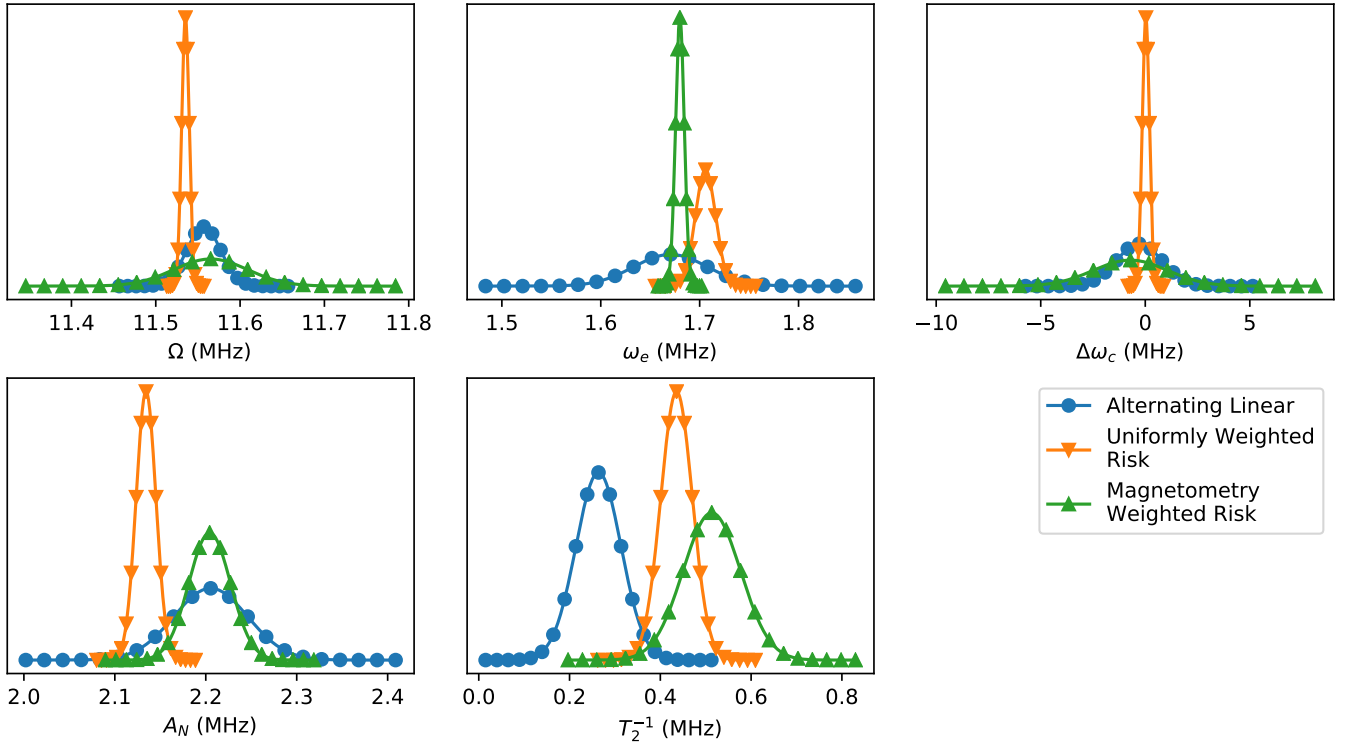


Figure 8: For each heuristic in Figure 5(a-c), posterior marginal distributions are plotted for the first (of 100) trials on each parameter relevant to the quantum dynamics of the system.

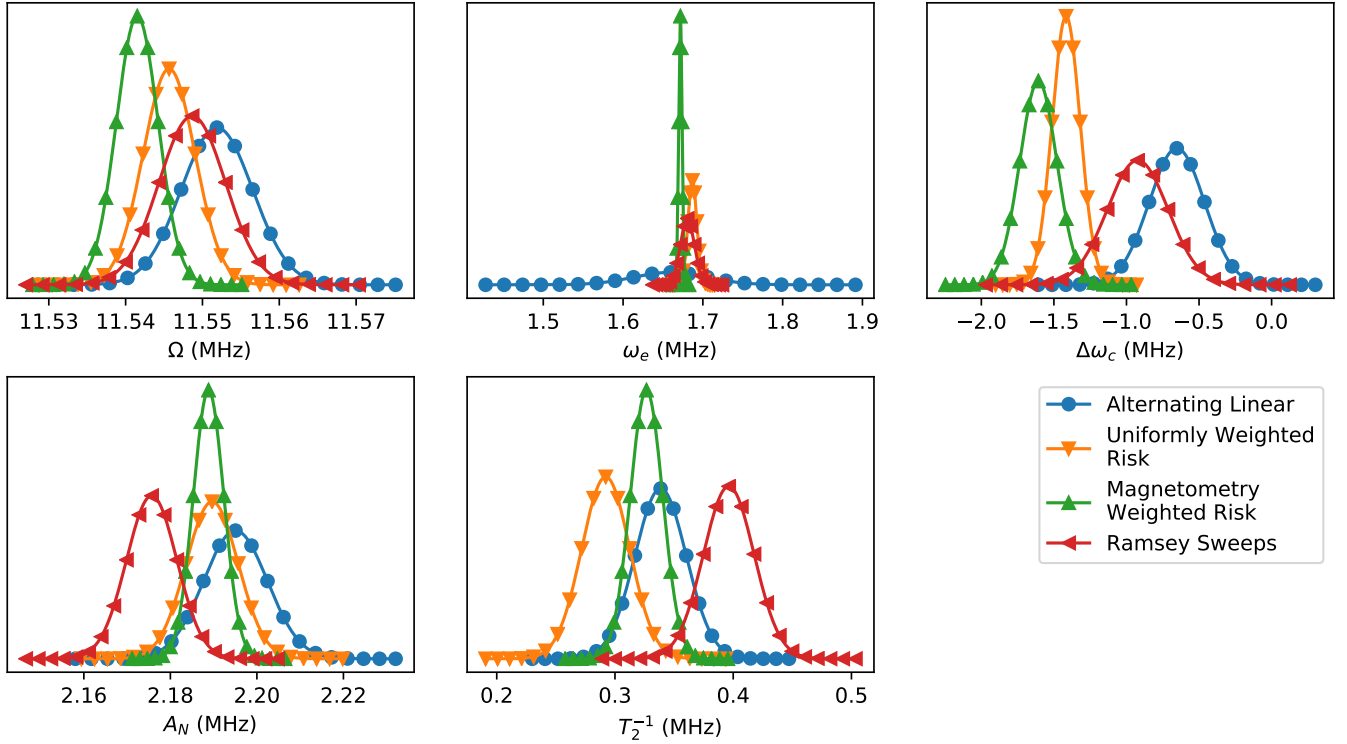


Figure 9: For each heuristic in Figure 5(d-f), posterior marginal distributions are plotted for the first (of 100) trials on each parameter relevant to the quantum dynamics of the system.

variables

$$\begin{aligned} X|\alpha &\sim \text{Poisson}(\alpha) \\ Y|\beta &\sim \text{Poisson}(\beta) \\ Z|\alpha, \beta, p &\sim \text{Poisson}(p\alpha + (1-p)\beta). \end{aligned} \quad (\text{B1})$$

The quantities  $\alpha$  and  $\beta$  are known as the bright reference and the dark reference, respectively. They are defined as the expected number of photons collected (and summed over  $N$  repetitions of the experiment) using the initial NV states  $|0\rangle$   $\langle 0|$  and  $|1\rangle$   $\langle 1|$ , respectively<sup>4</sup>.

The information content about  $p$  of this referenced Poisson model is not immediately obvious, and depends both on the magnitude of  $\alpha + \beta$ , as well as the contrast between  $\alpha$  and  $\beta$ . This is different than the strong measurement case mentioned above, where  $n$  strong measurements has a clear intuitive and operational interpretation. The goal of this section is to reduce information about the references  $\alpha$  and  $\beta$  into a single number with the same interpretation as  $n$ . This will allow one, for example, to quantitatively compare two experimental setups or NVs and decide which one is better at providing information about  $p$ .

It has been shown[40] that the Fisher information matrix of this referenced Poisson model is given by

$$J(p, \alpha, \beta) = \begin{pmatrix} \frac{(\alpha-\beta)^2}{p(\alpha-\beta)+\beta} & \frac{p(\alpha-\beta)}{p(\alpha-\beta)+\beta} & \frac{\alpha}{\beta+\alpha p-\beta p} - 1 \\ \frac{p(\alpha-\beta)}{p(\alpha-\beta)+\beta} & \frac{p^2}{p\alpha-p\beta+\beta} + \frac{1}{\alpha} & -\frac{(p-1)p}{p(\alpha-\beta)+\beta} \\ \frac{\alpha}{p\alpha-p\beta+\beta} - 1 & -\frac{(p-1)p}{p(\alpha-\beta)+\beta} & \frac{p\alpha+(p-2)(p-1)\beta}{\beta(p(\alpha-\beta)+\beta)} \end{pmatrix}, \quad (\text{B2})$$

with inverse matrix

$$J(p, \alpha, \beta)^{-1} = \begin{pmatrix} \frac{p(p+1)\alpha+(p-2)(p-1)\beta}{(\alpha-\beta)^2} & \frac{p\alpha}{\beta-\alpha} & \frac{(p-1)\beta}{\alpha-\beta} \\ \frac{p\alpha}{\beta-\alpha} & \alpha & 0 \\ \frac{(p-1)\beta}{\alpha-\beta} & 0 & \beta \end{pmatrix}. \quad (\text{B3})$$

Using the Cramer-Rao bound, these matrices let us estimate the information content of  $p$  in the referenced Poisson model. Specifically, they give us an estimate in each of the following extreme cases. First, the  $(p, p)$  element of  $J^{-1}$ ,  $(J^{-1})_{p,p} = \frac{p(p+1)\alpha+(p-2)(p-1)\beta}{(\alpha-\beta)^2}$ , is a lower bound on the variance of any (unbiased) estimate of  $p$  given that a single measurement of the triple  $(X, Y, Z)$  has been made, with no prior information about  $p$ ,  $\alpha$ , or  $\beta$  given. Second, the inverse of the  $(p, p)$  element of  $J$ ,  $(J_{p,p})^{-1} = \frac{p(\alpha-\beta)+\beta}{(\alpha-\beta)^2}$ , is a lower bound on the variance of any (unbiased) estimate of  $p$  given that a single measurement of  $Z$  has been made, assuming perfect knowledge of both  $\alpha$  and  $\beta$ .

It will be useful for us to also be able to interpolate between these two extremes, where some, but not all, prior information about  $\alpha$  and  $\beta$  is available. There are a few tacks that one might consider to achieve this, including the Bayesian Cramer-Rao bound, or looking directly at the risk of some estimator. Instead, we choose a slightly ad-hoc method as it actually produces a tractable calculation—statistics of the referenced Poisson model usually involve a triple infinite sum, and many calculations are simply not possible without numerics. To this end, let  $\sigma_\alpha^2$  and  $\sigma_\beta^2$  represent our prior variances of  $\alpha$  and  $\beta$ , respectively, before taking a measurement of  $Z|\alpha, \beta, p$ . We can now ask the question: how many times,  $M$ , we must measure  $X|\alpha$  and  $Y|\beta$  to produce these variances in the first place? We must allow  $M$  to depend on  $\alpha$  or  $\beta$  in each case. The distribution  $\text{Poisson}(M(\lambda)\lambda)$  has Fisher information given by  $\frac{(M(\lambda)+\lambda M'(\lambda))^2}{\lambda M(\lambda)}$ . Equating this to  $1/\sigma^2$  and solving the differential equation at  $M(0) = 0$  gives  $M = \lambda/4\sigma^2$ . Therefore consider the distribution

$$\text{Poisson}\left(\frac{\alpha^2}{4\sigma_\alpha^2}\right) \times \text{Poisson}\left(\frac{\beta^2}{4\sigma_\beta^2}\right) \times \text{Poisson}(p\alpha + (1-p)\beta) \quad (\text{B4})$$

which effectively results in our desired information about  $\alpha$  and  $\beta$ . Solving for the  $(p, p)$  element of the inverse Fisher information matrix of this distribution results in the formula

$$K = \frac{\beta + p\left(\alpha - \beta + p\sigma_\alpha^2 + (p-2)\sigma_\beta^2\right) + \sigma_\beta^2}{(\alpha - \beta)^2}. \quad (\text{B5})$$

---

<sup>4</sup> They are more accurately defined in terms of the pseudo-pure states that are actually created in the NV initialization procedure [40].

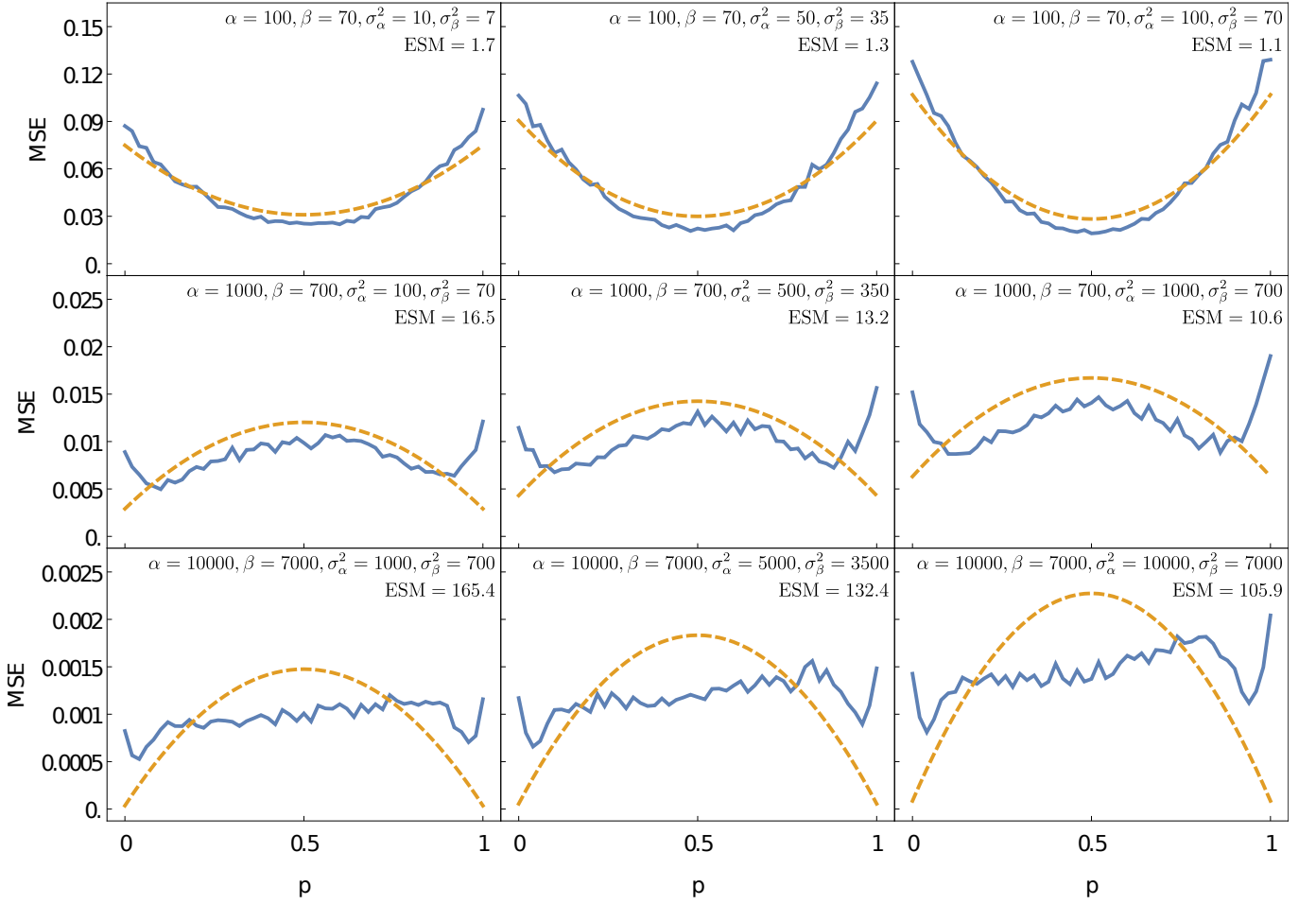


Figure 10: The mean-squared-error of the Bayes estimator is computed as a function of  $p$  for both the referenced Poisson model (blue, solid) and for a binomial model (orange, dashed) where  $n = \text{ESM}$ . The prior distribution on  $p$  is uniform. This is done in nine regimes, corresponding to the nine subplots of the figure. Each row uses a different magnitude of bright reference,  $\alpha$ , and each column uses a different amount of prior reference knowledge. The left column uses sub-Poisson error bars on  $\alpha$  and  $\beta$ , and the right column uses regular Poisson error bars.

This formula correctly interpolates between the case of perfect prior information, and prior information as collected by a single sample of  $(X, Y)|\alpha, \beta$ , namely,

$$\lim_{\sigma_\alpha^2, \sigma_\beta^2 \rightarrow 0} K = (J_{p,p})^{-1} \quad \text{and} \quad \lim_{\sigma_\alpha^2 \rightarrow \alpha, \sigma_\beta^2 \rightarrow \beta} K = (J^{-1})_{p,p}. \quad (\text{B6})$$

The inverse Fisher information of the binomial model  $\text{Binom}(n, p)$  is given by  $\frac{p(1-p)}{n}$ , which when integrated uniformly over  $[0, 1]$ , produces  $\frac{1}{6n}$ . Our definition for the number of effective strong measurements (ESM) of a referenced Poisson model with parameters  $(\alpha, \beta, \sigma_\alpha, \sigma_\beta)$  is defined by equating  $\int_0^1 K dp = \frac{1}{6n}$  and solving for  $n$ , which results in

$$\text{ESM} = \frac{(\alpha - \beta)^2}{3(\alpha + \beta) + 2(\sigma_\alpha^2 + \sigma_\beta^2)}. \quad (\text{B7})$$

This shows, for example, that having perfect information about  $\alpha$  and  $\beta$  before measuring  $Z|\alpha, \beta, p$  is roughly equivalent—in terms of information learned about  $p$ —to  $5/3 \approx 1.67$  times more effective strong measurements than the case where the triple  $(X, Y, Z)|\alpha, \beta, p$  is measured, but with no prior information.

Finally, in Figure 10, we use some numerics to show that the ESM quantity accurately relates the mean-squared error of the Bayes estimator for the referenced Poisson model and a binomial model with  $n = \text{ESM}$ .

### Appendix C: Brute-force Numerical Evaluation of Bayes Risk

Evaluating the full Bayes risk for continuous outcome probability distributions is not possible analytically apart from special cases such as linear models with a normal likelihood function. For finite outcome probability distributions the problem is more tractable, however as the number of possible outcomes grows to be large, or even infinite—such as the Poisson distributions considered within this paper—the evaluation once again becomes intractable.

The difficulty of evaluation is a result of the expectation taken in [Equation 7](#). For both infinite-discrete and continuous outcome probability distributions the expectation is intractable, however for finite discrete distributions, the expectation is a bounded discrete sum and straight-forward to evaluate numerically. We, therefore, aim to evaluate the Bayes risk by approximating the possible outcomes with a finite, discrete set of outcomes—note that this technique may also be used when the set of possible outcomes is finite but large enough to be computationally intractable. Typically, outcome domains are large with outcome probability mass concentrated to a small portion of the outcome domain. By fixing particle locations and sampling outcomes from these particles, we may evaluate the risk for only the outcomes that “matter” within the regions of outcome probability mass concentration.

We consider the case of evaluating the Bayes risk for the next experiment,  $e$ . We assume throughout this discussion, that this hypothetical experiment  $e$  was preceded by  $n$  experiments  $e_{1:n}$  with corresponding data  $d_{1:n}$ . In several places, for brevity of notation, we will omit conditioning on this prior information, for example, we have  $\Pr(d|e) = \Pr(d|e, d_{1:n}, e_{1:n})$ . We begin by re-approximating the particle filter prior distribution with a uniformly weighted particle distribution by sampling  $K'$  particles from the prior  $\pi_n$ ,

$$x_j \sim \pi_n(x), \quad (\text{C1})$$

which approximates the prior  $\pi_n$  as

$$\pi_n(x) \approx \frac{1}{K'} \sum_i^{K'} \delta(x - x_i). \quad (\text{C2})$$

For each particle we now sample a datum from the likelihood function,

$$d^{(j)} \sim L(x_j; d, e) \quad \forall x_j \in x_{1:K'}. \quad (\text{C3})$$

The set of sampled data is an approximation to the joint outcome, particle distribution

$$\Pr(d, x|e) \approx \frac{1}{K'} \sum_i^{K'} \delta(d - d^{(i)}) \delta(x - x_i). \quad (\text{C4})$$

The average utility—[Equation 4](#)—may be expanded in conjunction with [Equation 3](#) as

$$\begin{aligned} U_n(e) &= \int \int \Pr(d|x, e) \tilde{\pi}_{n,d,e}(x) U_n(x, d, e) dx dd \\ &= \int \int \Pr(d, x|e) U_n(x, d, e) dx dd. \end{aligned} \quad (\text{C5})$$

The approximate particle, datum joint distribution, [Equation C4](#) may be substituted into [Equation C5](#) and the integrals are thus replaced by a sum,

$$U_n(e) \approx \frac{1}{K'} \sum_i^{K'} U_n(x, d, e), \quad (\text{C6})$$

which is the average utility of the joint sampled particle, datum distribution. When the utility is the negative mean-squared error the Bayes risk has the approximate form

$$r_{n,Q}(e) \approx \frac{1}{K'} \sum_i^{K'} \text{Tr} Q(x_i - \hat{x}_{n,d^{(i)},e})^T (x_i - \hat{x}_{n,d^{(i)},e}), \quad (\text{C7})$$

where  $\hat{x}_{n,d^{(i)},e}$  is the posterior mean given the the approximate prior [Equation C2](#),

$$\hat{x}_{n,d^{(j)},e} = \sum_i^{K'} \frac{L(x_i; d^{(j)}, e)}{K'} x_i. \quad (\text{C8})$$

The evaluation of the Bayes risk requires on the order of  $O(K'^2)$  likelihood evaluations. However, typically a large number of outcome samples will be required to effectively sample the outcome domain of each particle and the total number of outcome samples will roughly be  $O(Kn_d)$ , where  $n_d$  is roughly the average number of outcome datum desired per particle. This may be prohibitively large when sampling is expensive.

Provided the outcome domain does not depend on the experiment—as is the case for our experiments—we may perform maximum importance sampling (MIS) to sample outcomes from an alternative distribution—chiefly the marginalized outcome distribution  $\Pr(d|e)$ —and properly re-weight the resultant utility functions [48]. The sampled outcome distribution  $\Pr(d|e)$  is obtained from the sampled  $\Pr(d, x|e)$  by neglecting the associated model parameter,

$$\Pr(d|e) \approx \frac{1}{K'} \sum_i^{K'} \delta(d - d^{(i)}). \quad (\text{C9})$$

The MIS utility is given as

$$\begin{aligned} U_n(e) &= \int \int \Pr(d|x, e) \pi_n(x) \frac{\Pr(d|e)}{\Pr(d|e)} U_n(x, d, e) dx dd \\ &\approx \frac{1}{K'} \sum_i^{K'} \sum_j^K \frac{\Pr(d^{(i)}|x_j, e) \omega_{n,j}}{\Pr(d^{(i)}|e)} U_n(x_j, d^{(i)}, e) \\ &= \frac{1}{K'} \sum_i^{K'} \sum_j^K \omega_{n+1|d^{(i)},j} U_n(x_j, d^{(i)}, e), \end{aligned} \quad (\text{C10})$$

where the judicious choice of the sampling distribution has allowed the utility to be written as the average of the posterior utility expectation over the marginalized outcome distribution. For the case of the Bayes risk this may be further simplified to

$$\begin{aligned} r_{n,Q}(e) &\approx \frac{1}{K'} \sum_i^{K'} \text{Tr} \left[ Q \text{Cov}_{\tilde{\pi}}[x|d^{(i)}, e] \right] \\ &= \frac{1}{K'} \sum_i^{K'} \text{Tr} \left[ Q(\widehat{x^T x}_i - \widehat{x}_i^T \widehat{x}_i) \right], \end{aligned} \quad (\text{C11})$$

where  $\widehat{x^T x}_i = \sum_j^K \omega_{n+1|d^{(i)},j} x_j^T x_j$ , and  $\widehat{x}_i = \sum_j^K \omega_{n+1|d^{(i)},j} x_j$ .

In general the the initial prior distribution may be down-sampled to some number of particles  $K$ , such that we now have two parameters that may be tuned, the number of outcome samples  $K'$ , and the number of model parameter particles  $K$ . With the MIS Bayes risk, the number of likelihood function calls is now  $O(KK')$ , with only  $O(K')$  outcome samples required. We utilize the MIS Bayes risk for experiment design within this paper.

In practice a trade-off between accuracy and computational cost/time is necessary when selecting the number of outcomes and particle samples,  $K'$  and  $K$  respectively for the evaluation of the MIS Bayes risk. A comparison of various sampling numbers is displayed in the heatmaps of [Figure 11](#), which were evaluated with the wide prior of [Equation 20](#) and experiments for the uniformly weighted Bayes risk experiment design heuristic given in [Table I](#). The aquisition of 4000 ESM takes roughly 10 seconds, as the full particle filter update of 30000 particles takes roughly 2 seconds, there are 8 seconds remaining in which to compute the Bayes risk and select the optimal experiment. We use  $K' = 512$  outcome samples and  $K = 1024$  particle filter samples, as this strikes a balance between accuracy while keeping the evaluation time below our threshold on our computational hardware. As this problem is massively parallel, if desired it is simple to use additional computational resources to refine to the evaluation accuracy.

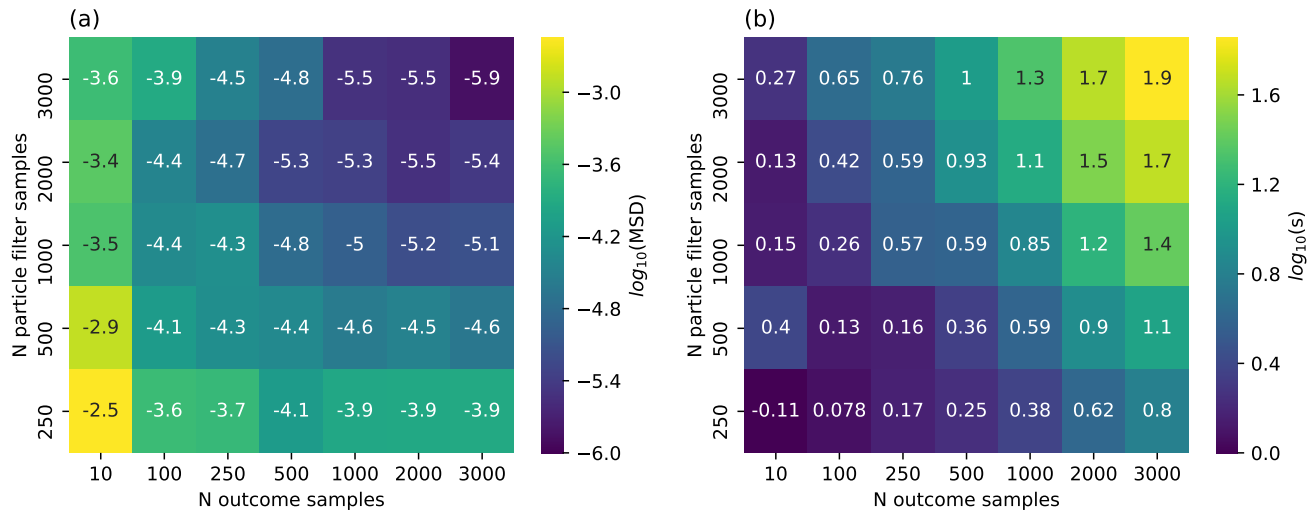


Figure 11: Comparison of various outcomes and particle sampling accuracies and times when evaluating the MIS Bayes risk. The prior distribution over model parameters is given by Equation 20, and the experiments which the Bayes' risk is computed for is the uniformly weighted experiment design risk heuristic found in Table I. (a) Log mean squared difference for all experiments computed with respect to a 4000 outcome, 4000 particle reference evaluation. (b) Log evaluation time(s) of Bayes risk over all experiments for a given number of outcome and particle samples. These calculations were done on an i9-7980XE CPU.